WM25

19th International Symposium of Ballistics, 7–11 May 2001, Interlaken, Switzerland

ROLE OF TEXTURE IN SPIN FORMED Cu SHAPED-CHARGE LINERS

A.J. Schwartz[1], M.J. Busche[2], R. Becker[1], M. Kumar[1], and D.J. Nikkel[1]

[1]Lawrence Livermore National Laboratory, 7000 East Ave, Livermore, CA 94550, USA
[2]Mechanical Engineering Department, MIT, Cambridge, MA, 02139, USA

Spin formed Cu shaped charge liners are known to produce a rotating jet and are used for the spin compensation effect. The causes of spin compensation can be mechanical in nature or can be grounded in microstructural issues such as texture, residual stress, grain size, and morphology variations. This investigation focuses on determining specific microstructural parameters that influence jet rotation and modeling the jet formation process using anisotropic plasticity in a 3-D finite element framework. The experimental texture has been mapped onto a finite element grid for 3-D modeling to obtain the normal-shear deformation coupling information needed to construct a plastic flow potential. Simulations of a collapsing ring and extending rod demonstrate rotation.

INTRODUCTION

Spin formed Cu shaped charge liners have been shown to produce a rotating jet and are used for the spin compensation effect. The rotational velocity was experimentally measured by Winer et al. using a high-resolution image-converter camera [1]. Early studies by Gainer and Glass [2] and Glass et al. [3] of shear-formed liners suggested residual stress or anisotropy as possible causes of spin compensation. This anisotropy can be mechanical in nature or can be grounded in microstructural issues such as texture, residual stress, grain size, and morphology variations. Chou and Segletes [4] modeled the jet rotation with an analytical model and finite-element code in two-dimensions. The source of rotation in their study was microstructure-induced anisotropy in the form of normal-shear coupling where applied stress can induce a shear in an orthogonal direction. Normal-shear coupling based on the measured crystallographic texture provides the driving force for the rotation in the present study.

Variations in texture were traditionally studied by X-ray diffraction techniques, but this has the disadvantage of an indirect correlation with the actual microstructure. With the advent of scanning electron microscopy-based electron backscatter diffraction (EBSD), it is now possible to make a direct comparison between texture components and their spatial location in the microstructure. This investigation focuses on determining specific microstructural parameters that influence jet rotation and modeling the jet formation

process using anisotropic plasticity in a 3-D finite element framework. The experimental texture in the form of the orientation distribution function has been mapped onto a finite element grid for 3-D modeling to obtain the normal-shear deformation coupling information needed to construct a plastic flow potential. This flow potential was used in 3-D simulations of a collapsing ring and a stretching rod.

RESIDUAL STRESS MEASUREMENTS

Residual stresses were determined by neutron scattering at various points along the wall of the liner. The stress components at the mid-wall position, shown in Table 1, reveal that the normal stresses are small, but the in-plane stresses are quite high. The residual stresses are not included in these initial calculations, but are available for implementation at a later date.

Table 1: Neutron diffraction measurements of the residual stress at the mid-wall.

Position	σ'_{11} (MPa) Thickness	σ'_{22} (MPa) Circumferential	σ_{33} (MPa) Longitudinal
A (near apex)	5 ± 35	-16 ± 35	22 ± 35
B	-55 ± 35	105 ± 35	28 ± 35
C	27 ± 35	-103 ± 35	16 ± 35
D	-3 ± 35	-67 ± 35	-6 ± 35
E (near base)	72 ± 35	-53 ± 35	12 ± 35

MICROTEXTURE DETERMINATION

Detailed EBSD measurements were performed to evaluate the change in microtexture from the apex to the base as well as through the thickness of the liner. A pole figure, which represents the texture 0 to 260 microns from the inner surface at a location near the apex of the liner, is shown in Fig. 1. The (100) pole figure reveals that the strongest texture component is aligned 45° to the axis that runs from the apex to the base and is a result of shear deformation due to the spin forming process.

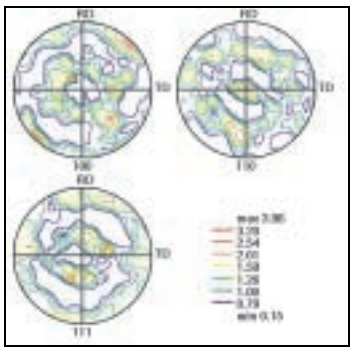

Figure 1: Pole figure obtained from EBSD near apex, inner surface, 0-260 μm depth. ND is normal to the outer surface of the cone, RD runs from the apex to the base, TD is circumferential to the surface.

CONSTRUCTION OF A REPRESENTATIVE VOLUME ELEMENT

The motivation behind the detailed characterization of the shaped charge liner is to enable the creation of a 3-D representative volume element (RVE) model for the polycrystalline material which can be queried to provide property information consistent with the measured microstructure. To accomplish this, salient characteristics of the microstructure (orientation and grain volume fraction) need to be extracted from the section data and used to construct a plausible 3-D polycrystal geometry.

The data obtained from EBSD analysis of the shaped charge liner was run through a clean-up procedure available in the TSL [5] software to eliminate points with low confidence indices. Individual orientations were then associated with particular grains based on proximity and misorientation from neighboring points. This created a set of grains to be used in constructing the RVE.

The 3-D RVE to be constructed is a cube comprised of grains. Since the finite element analysis requires each hexahedral finite element to be of only one orientation, it is conceptually straightforward to imagine that the representative volume is divided into a regular array of finite elements, each assigned an orientation based on its location in the 3-D grain structure. However, arriving at this configuration is not trivial since grains of specified volumes must be assembled in a manner that fills space.

The representative volume is constructed by creating virtual grains of specified volumes, combining them in a finite size box, rearranging the grains to minimize overlap and gaps, and finally eliminating any overlaps and filling all gaps [6]. The initial grains are constructed by assembling sets of identical small cubes into clusters. The number of cubes in each cluster is proportional to the volume of the grain. The total number of cubes used in constructing the clusters is chosen to be approximately 30% more than the targeted number of elements for the finite element analysis. The clusters are placed in the space defining the RVE on a lattice corresponding to the finite elements. Initially there are overlapping elements and gaps. The clusters are then randomly either moved a step or rotated 90° about one of the orthogonal coordinate directions. If the configuration is improved, in terms of overlaps and gaps, the change is accepted. Otherwise, it is either accepted or rejected based on a probability function that decreases in time.

When the configuration has stabilized, lattice orientations associated with each cube cluster are assigned to the corresponding elements of the finite element model. If more than one cube occupies an element, the last cube to move to that location is chosen. For the small number of empty elements that remain, the orientation of a randomly chosen neighboring element is assigned. A representative volume element created by this technique is shown in Fig. 2.

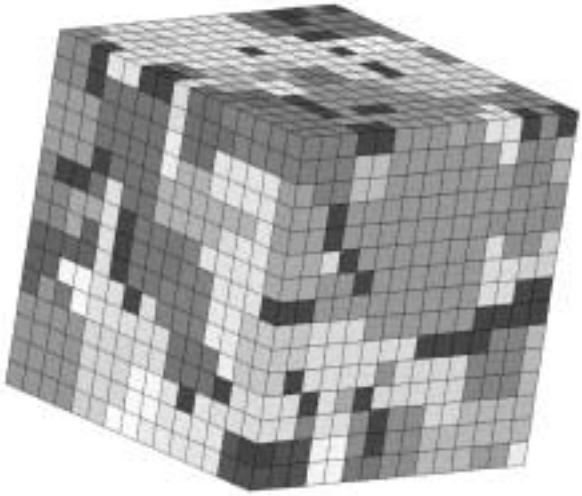

Figure 2: Example of a representative volume element reconstructed from EBSD data.

EVALUATION OF MATERIAL ANISOTROPY

The mechanical response of each zone of the polycrystal representative volume element is determined through use of a crystal plasticity finite element model which accounts for deformation by slip on prescribed slip systems. The elastic-visco plastic model fully accounts for finite deformation and reorientation of the crystal lattice with strain. The implementation in ALE3D [7] is identical to the ABAQUS/Standard [8] implementation [9] which has been used extensively for both single and polycrystal analyses of FCC materials [10,11].

The crystal elastic constants and slip system hardening were chosen to be consistent with copper. Slip was assumed to occur exclusively on the twelve {111}<110> slip systems, and Taylor hardening was assumed where all slip systems have the same strength. Since the result of interest from the numerical analyses is the anisotropic response of the RVE at modest strains (15%), neither the elasticity nor the particular form for the strain hardening have a significant impact on the results. The assumption of equal interaction among the slip systems, the Taylor assumption, will affect the anisotropy predictions.

The particular information which needs to be extracted from the polycrystal RVE is how the material deforms when subjected to stress. In simplest form, one can assume that the direction of the plastic strain rate tensor, $\mathbf{d}^p$, is a linear function of the stress deviator tensor,σ':

$$\mathbf{d}^p = \lambda \mathbf{K} : \sigma' \tag{1}$$

K is a constant fourth order tensor mapping the stress direction to the strain rate direction, and λ is a factor that adjusts the magnitude of the strain rate. Under the assumption that plastic flow occurs in a direction normal to the yield surface (normality flow rule), this

linear form is consistent with a generalized von Mises yield function with a yield surface, ϕ, defined as,

$$\phi = \sqrt{\frac{3}{2}\,\sigma' : \mathbf{K} : \sigma'} - \bar{\sigma} \tag{2}$$

where $\bar{\sigma}$ is the equivalent flow strength of the material. If **K** were equal to the identity tensor, the yield surface and plastic flow model would be identical to classical J_2-flow theory.

The goal of the analyses on the representative volume element is to determine the fourth order tensor **K**. If eq. (1) is written in matrix form where both the stress and plastic strain rate are represented by vectors of length 6, the *K* matrix has 21 entries to be determined. To ensure that all potential deformation couplings are sampled when exercising the RVE, six independent calculations are performed. These are isochoric extensions in the three coordinate directions and three pure shear deformations in orthogonal planes. The six resultant stress components for the RVE are determined for each simulation by averaging the stress components of the elements.

The result of these simulations is the stress as a function of total strain rate. However, eq. (1) requires the plastic part of the strain rate. Using the additive decomposition of the strain rate into elastic and plastic parts and employing Hooke's law relating the stress rate to the elastic strain rate, an expression giving the plastic part of the strain rate is,

$$\mathbf{d}^{\mathrm{p}} = \mathbf{d} - \mathbf{d}^{\mathbf{e}} = \mathbf{d} - \mathbf{C} : \dot{\sigma} \tag{3}$$

where **C** is the elastic compliance tensor for the RVE. The elastic compliance tensor is computed from the data obtained from the calculations on the RVE prior to the onset of plasticity where the total strain rate equals the elastic strain rate.

Each of the six calculations gives six equations for the 21 unknowns of **C**. In matrix form, *C* is written as a vector of 21 unknowns, $\dot{\sigma}$ is a 6 x 21 matrix of the stress components and d^{e} is a vector of the 6 prescribed strain rate components.

$$\left[\,\dot{\sigma}\,\right]\{\mathrm{C}\} = \left\{\mathrm{d}^{\mathrm{e}}\right\} \tag{4}$$

The key to the procedure lies in constructing the 6 x 21 $\dot{\sigma}$ matrix which contains a large number of zeros. The results of the six simulations are combined to produce a set of 36 equations for the 21 unknowns. *C* remains a vector of 21 unknowns, d^{e} is a vector of 36 applied strains and $\dot{\sigma}$ is a 36 x 21 matrix.

A "least squares" solution for this over determined system of equations is obtained by applying the singular valued decomposition method to the $\dot{\sigma}$ matrix to obtain a pseudo inverse. This pseudo inverse is applied directly to eq. (4) to determine the 21 components of the *C* matrix.

With *C* known, it can be combined with the applied strain rate and stress rate calculated from the RVE to obtain the plastic strain rate from eq. (3). Equation (1) can then placed in a form similar to eq (4) and solved for the components of *K* employing the singular valued decomposition method and the same procedure outlined above.

The K matrix determined from the crystal orientation data shown in Fig. 1 is given by

$$K = \begin{bmatrix} 0.525 & . & . & . & . & . \\ -0.262 & 0.543 & . & . & \textit{symmetric} & . \\ -0.263 & -0.281 & 0.544 & . & . & . \\ -0.015 & -0.005 & 0.020 & 0.490 & . & . \\ 0.001 & -0.005 & 0.004 & 0.011 & 0.485 & . \\ 0.012 & -0.023 & 0.011 & 0.008 & 0.014 & 0.502 \end{bmatrix} \tag{5}$$

The nine entries in the lower left of the matrix represent normal-shear coupling where stress applied normal to one of the faces of the RVE will cause a shear deformation. If the material were isotropic or orthotropic, these entries would be zero. If the texture had stronger non-orthotropic components, these terms would be larger and the predicted rotation greater.

RESULTS USING THE CALCULATED MATERIAL ANISOTROPY

To determine if material anisotropy could induce the spinning behavior seen in a spin formed shaped charge, two sets of sample calculations were performed using the generalized von Mises yield function described by eqs. (1) and (2) with either isotropic properties or the K matrix given by eq. (5). The first example is of a ring collapsing under applied pressure. This is representative of the initial deformation of the shaped charge liner. The second example is the stretching of a hollow tube. This is reminiscent of the extension of the formed jet.

The ring for the collapse calculation was 40 mm ID and 3 mm long with a 0.3 mm wall thickness. The faces of the ring were constrained such that the length of the ring along its axis remained fixed. The initial and final ring shapes are superimposed in Fig. 3a. Magnified views of the deformed ring for the isotropic and anisotropic material properties are given in Figs. 3b and 3c, respectively. It is noted that the calculation performed with the anisotropic material properties produced a longitudinal spin whereas no such spin is noted for the isotropic material.

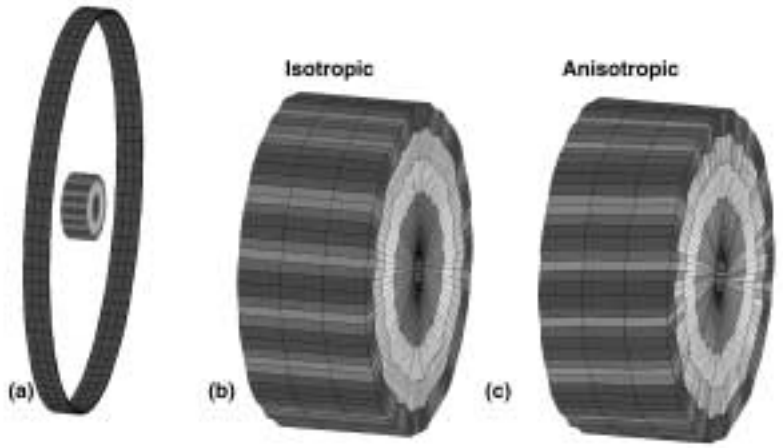

Figure 3. Illustration of anisotropy induced twisting in a collapsing ring.

The stretching calculation started with a 40 mm ID ring which was 50 mm long with a 1 mm wall thickness. The cylinders were stretched to approximately 10 times their initial length. As with the collapsing ring, the stretching tube made of anisotropic material (Fig. 4b) deformed with a twist while the calculation using isotropic properties (Fig. 4a) showed stretching without a twist.

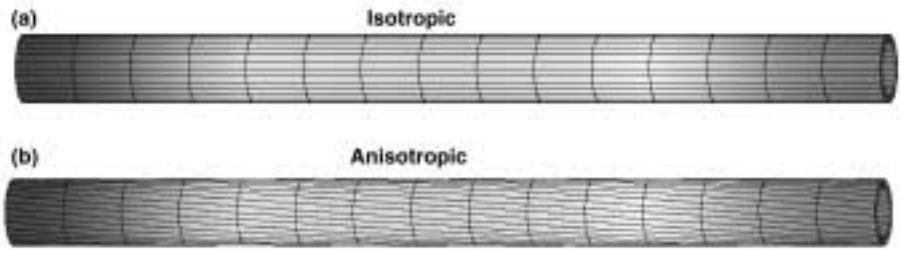

Figure 4: Illustration of anisotropy induced twisting in a stretched cylinder.

CONCLUSIONS

Anisotropic material properties determined from the measured crystallographic texture of a copper shaped charge liner exhibit a normal-shear coupling which manifests itself as a twisting deformation in simulations of a collapsing ring or a stretching rod. Based on these results, it is anticipated that full 3-D simulations of a shaped charge using these anisotropic properties will also produce a twist. These results support the hypothesis that the spin compensation of a spin formed shaped charge liner may be produced by the changes in crystallographic texture induced during the spin forming operation.

ACKNOWLEDGMENTS

The authors acknowledge the support of the Joint DoD/DOE Munitions Technology Development Program. This work was performed under the auspices of the U.S. Department of Energy by the University of California, Lawrence Livermore National Laboratory under Contract No. W-7405-Eng-48.

REFERENCES

1. K. Winer, L. Shaw, S. Muelder, D. Breithaupt, and D. Baum, "Dynamic Behavior of a Shear-Formed Shaped-Charge Liner", *Propellants, Explosives, Pyrotechnics 18* 345–351 1993
2. M.K. Gainer, and C.M. Glass, "A study of Metallurgical Effect in High Velocity Deformation of Copper Using Rotary Extruded Liners", *BRL Report 1167* May 1962
3. C.M. Glass, M.K. Gainer, and G.L. Moss, "Effects of Anisotropies in Rotary Extruded Liners", *BRL Report 1084* November 1959.
4. P.C. Chou and S.B. Segletes, "Jet Rotation Resulting From Anisotropy of Shaped-Charge Liners", *11th International Symposium on Ballistics*, Brussells, May 9–11, 1989
5. Orientation Imaging Microscopy Software Users Manual, TSL Inc. Draper, UT, 1999
6. M.J. Busche "K, the Fourth Order Coefficient Tensor Used in ALE3D's Quadratic Generalized von Mises Yield Function, in Five Easy Steps", *Lawrence Livermore National Laboratory Report, UCRL-ID-140135*, August 2000
7. R. Couch, R. Sharp, I. Otero, R. Tipton and R. McCallen, "Applications of ALE Techniques to Metal Forming Simulations," in Advanced Computational Methods for Material Modeling, D.J. Benson and R.J. Asaro eds., ASME AMD Vol. 180, New York, NY, 133–140, 1993
8. ABAQUS Users' Manual, Hibbitt, Karlsson & Sorensen, Inc., Pawtucket, RI
9. R.E. Smelser and R. Becker, "ABAQUS User Subroutines for Material Modeling", *ABAQUS Users' Conference, Stresa Italy*, Hibbitt, Karlsson & Sorensen, Providence, RI, 207–226, 1989
10. R. Becker, J.F. Butler Jr., H. Hu, and L.A. Lalli, "An Analysis of an Aluminum Single Crystal with Unstable Initial Orientation (001)[110] in Channel Die Compression", *Metall. Trans A. 22A* 45–58 1991
11. R. Becker "Effects of Strain Localization on Surface Roughening During Sheet Forming", *Acta Mater. 46* 1385–1401 1998